J Biomol NMR (2016) 64:75–85
DOI 10.1007/s10858-015-0009-6

ARTICLE

An encodable lanthanide binding tag with reduced size and flexibility for measuring residual dipolar couplings and pseudocontact shifts in large proteins

Adam W. Barb[1] · **Ganesh P. Subedi**[1]

Received: 27 October 2015 / Accepted: 28 December 2015 / Published online: 4 January 2016

Abstract Metal ions serve important roles in structural biology applications from long-range perturbations seen in magnetic resonance experiments to electron-dense signatures in X-ray crystallography data; however, the metal ion must be secured in a molecular framework to achieve the maximum benefit. Polypeptide-based lanthanide-binding tags (LBTs) represent one option that can be directly encoded within a recombinant protein expression construct. However, LBTs often exhibit significant mobility relative to the target molecule. Here we report the characterization of improved LBTs sequences for insertion into a protein loop. These LBTs were inserted to connect two parallel alpha helices of an immunoglobulin G (IgG)-binding Z domain platform. Variants *A* and *B* bound Tb^{3+} with high affinity (0.70 and 0.13 μM, respectively) and displayed restricted LBT motion. Compared to the parent construct, the metal-bound *A* experienced a 2.5-fold reduction in tag motion as measured by magnetic field-induced residual dipolar couplings and was further studied in a 72.2 kDa complex with the human IgG1 fragment crystallizable (IgG1 Fc) glycoprotein. The appearance of both pseudocontact shifts (−0.221 to 0.081 ppm) and residual dipolar couplings (−7.6 to 14.3 Hz) of IgG1 Fc resonances in the IgG1 Fc:(variant *A*:Tb^{3+})$_2$ complex indicated structural restriction of the LBT with respect to the Fc. These studies highlight the applicability of improved LBT sequences with reduced mobility to probe the structure of macromolecular systems.

✉ Adam W. Barb
abarb@iastate.edu

[1] Roy J. Carver Department of Biochemistry, Biophysics and Molecular Biology, Iowa State University, 2214 Molecular Biology Building, Ames, IA 50011, USA

Keywords Immunoglobulin G · Glycoprotein · Terbium luminescence · PCS · RDC

Introduction

Metal ions exhibit important properties that assist characterization of macromolecular structure and motion. The high electron density of many metals provides unambiguous signals in X-ray diffraction data that can be used to determine phases (Silvaggi et al. 2007). Paramagnetic metals can be observed directly, as contrast reagent, or reveal a wealth of information regarding the structural and dynamic features of macromolecules using electron paramagnetic resonance, magnetic resonance imaging or nuclear magnetic resonance (NMR) spectroscopy (Hiruma et al. 2013; Iwahara and Clore 2006; Pilla et al. 2015; Shulman et al. 1969; Skinner et al. 2015; Tolman et al. 1995). Long distance restraints (5–50 Å) from measurements of paramagnetic effects are invaluable to refining molecular models built from short-range nuclear Overhauser effects (NOEs, <6 Å) and complementary solution NMR spectroscopy data (Bertini et al. 2002).

Paramagnetic metals can occur naturally in a macromolecule (Butler 1998; Sjodt et al. 2015) or be introduced by replacing an existing metal (Keniry et al. 2006), covalently or non-covalently added as a chelate (Huang et al. 2013; Lee et al. 2015; Loh et al. 2015; Wei et al. 2013; Yang et al. 2015), bound by an unnatural amino acid (Loh et al. 2013; Park et al. 2015), or lanthanide-binding peptide sequence tag (LBT) engineered into the protein sequence (Barthelmes et al. 2011; Feeney et al. 2001; Gaponenko et al. 2000; Martin and Imperiali 2015; Nitz et al. 2003; Su et al. 2008), to reference a few key examples. One common limitation to artificial tags is the presence of metal ion

motion. Modeling motion as an additional variable in structure calculations has proven effective with paramagnetic probes including the non-metallic nitroxide spin label and EDTA-Mn(II) complexes (Iwahara et al. 2004a, b). For incorporating metals, polypeptide-based tags have the advantage of ease-of-use by simple encoding into a protein expression vector but predicting tag motion for structure calculations is challenging due to an increase in tag size (~1800 Da) and number of rotatable bonds when compared to the nitroxide labels (~170 Da). Engineering proteins to attach LBTs within the protein rather than at the N or C termini has proven successful, either through incorporation into a loop connecting two defined secondary structural elements or through secondary attachment to a cysteine residue (Barb et al. 2012; Barthelmes et al. 2011; Saio et al. 2009). Such alterations likely will reduce, but not eliminate, peptide-based tag motion. We sought to improve existing LBT sequences by eliminating unnecessary amino acids that contribute to neither conformational stability nor lanthanide binding.

Paramagnetism from unpaired electrons introduces a strong local magnetic field that increases relaxation rates of nearby nuclei with an r^{-6} distance dependence (paramagnetic relaxation enhancement, or PRE) or perturbs resonance frequencies with an orientation and r^{-3} distance dependence (pseudocontact shifts, or PCSs) in NMR spectra (reviewed in Koehler and Meiler 2011; Otting 2008). One advantage of these phenomena is that they are measurable using only 1*d* or 2*d* NMR experiments.

Paramagnetic lanthanide ions are becoming increasingly utilized as structural probes because of their limited chemical reactivity, bioorthogonal nature, similar coordination chemistry across the group, and strong magnetic properties. The magnetic susceptibility (χ)-tensor for most paramagnetic lanthanide ions is characterized by significant anisotropy that leads to partial alignment of lanthanide chelates in a magnetic field and, as an independent phenomenon, PCSs of resonances (Otting 2008). Anisotropy is greatest for the Tb^{3+}, Dy^{3+} and Tm^{3+} ions. Though paramagnetic, Gd^{3+} has an isotropic χ-tensor and does not cause alignment or PCSs. The diamagnetic lanthanide ions La^{3+} and Lu^{3+} are useful in control experiments because they neither align nor cause PCSs and PREs.

Partial alignment of a paramagnetic molecule reintroduces residual dipolar couplings (RDCs) that can be used as a powerful mechanism to measure molecule alignment. RDCs are not normally observed in solution NMR experiments due to rapid isotropic tumbling that causes dipolar couplings to average to zero. The coupling strength is related to the distance between two nuclei and their average orientation with respect to the static magnetic field, thus it is possible to measure the angles between different internuclear vectors in a molecule (Prestegard et al. 2004). The strength of molecular alignment is reflected in the strength of residual dipolar couplings (RDCs) (Koehler and Meiler 2011; Otting 2008 and references therein). Larger RDC values and a larger principle alignment tensor (Da) of the alignment indicate a greater degree of alignment. Furthermore, RDCs contribute high-resolution information relating relative domain orientations of multi-domain macromolecules.

Paramagnetic probes are particularly applicable to structural investigations of large systems by solution NMR spectroscopy where molecular mass combined with limited labeling options or conformational exchange favors sparse amino acid labeling and prohibits many modern 3*d* and 4*d* experiments to measure long-range through-space and through-bond nuclear interactions (Otting 2008; Yagi et al. 2013). One such system of interest is the Fragment crystallizable (Fc) region of immunoglobulin G1 (IgG1). IgG1 Fc is a homodimer with a single N-glycan at Asn297 that is critical to Fc γ receptor mediated immune cell activation (Hanson and Barb 2015) and glycan composition is strongly correlated with rheumatoid arthritis disease (Parekh et al. 1985). As a result of the post-translational modification, active IgG1 Fc can only be produced in mammalian cells that do not permit deuterium labeling during expression. To probe the IgG1 Fc structure in solution, a chimeric Fc and lanthanide-binding protein was designed based upon three helices of the Fc-binding Z-domain (Nilsson et al. 1987; Tashiro et al. 1997) and a lanthanide-binding tag (LBT) (Nitz et al. 2003; Su et al. 2006), termed Z-l2LBT (Barb et al. 2012). Despite replacing loop 2, connecting helices 2 and 3 of the Z-domain, with the LBT, considerable tag motion was observed (Fig. 1).

Here we present the improvement of one polypeptide-based LBT to reduce motion and preserve affinity towards lanthanide ions. Though LBT sequences are applicable to numerous types of techniques, we utilized solution NMR spectroscopy to provide a high-resolution and quantifiable characterization of protein structure and motion. Two variants with reduced loops linking the Z domain to the LBT were prepared and characterized. We also investigated the utility of one design to probe the structure of a large 72.2 kDa complex with IgG1 Fc.

Experimental conditions

Materials

All materials, unless otherwise noted, were from Sigma-Aldrich. Stable isotope-enriched compounds were purchased from Cambridge Isotopes.

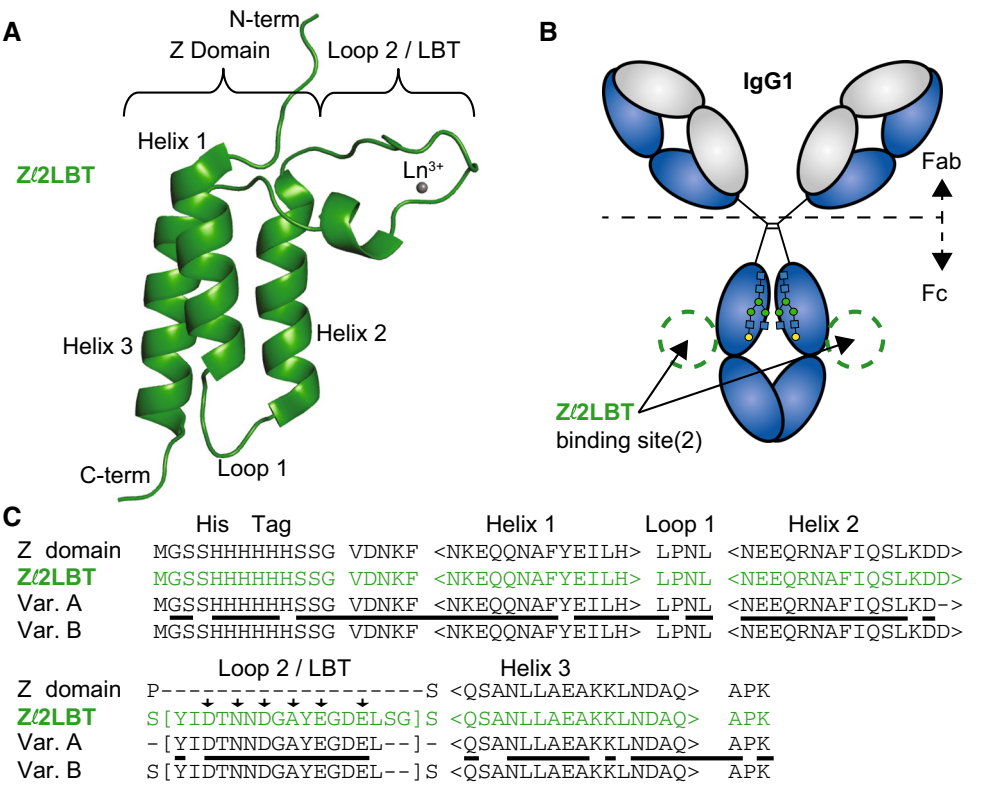

Fig. 1 Features of chimeric IgG and lanthanide-binding Z domain designs. **a** A *green ribbon* diagram depicts the Z domain with a lanthanide binding tag in loop 2 (Z-l2LBT) (Barb et al. 2012). **b** Z-l2LBT binds to the same surface of IgG1 Fc as the parent Z-domain. **c** Variant *A* and *B* differ from the parent Z-l2LBT protein by removal of 5 and 2 residues from the LBT/Z linker, respectively. *Arrows* indicate LBT residues that directly interact with Ln^{3+} ions. *Underlining* of the variant *A* sequence denotes assigned amide resonances

Protein expression and characterization

Z-l2LBT expression using *E. coli* BL21* cells was described previously (Barb et al. 2012). Open reading frames for variants *A* and *B* were synthesized (Genscript) and cloned into pET29 as described for the Z-l2LBT construct (Barb et al. 2012). Expression, stable isotope labeling, purification, and Tb^{3+} binding measurements of variants *A* and *B* were performed as previously described (Barb et al. 2012). A modified construct of variant *A* was prepared that permitted tobacco etch virus protease (TEV)-catalyzed cleavage of the His tag (liberating $G^{13}V^{14}D^{15}…K^{83}$) for studies of the Fc:*A* complex. The TEV reaction was performed at 25 °C for 16 h in the dark in a buffer containing 50 mM trisaminomethane, 100 mM sodium chloride, 0.5 mM ethylenediaminotetraacetic acid and 2 mM beta-mercaptoethanol, pH 8.2. The cleaved variant *A* product was isolated by passing the reaction mixture over a Ni–NTA column (Qiagen) and collecting the flow-through fraction. Cleaved variant *A* (1 mL) was then subject to dialysis for 4 h against 1 l of 25 mM 3-(N-morpholino)propanesulfonic acid (MOPS), 100 mM potassium chloride at 25 °C using a 3000 molecular weight-cutoff dialysis tubing (Spectrum Labs). The dialysis was repeated against a fresh 1 l of the same MOPS buffer.

Expression and purification of the human IgG1 Fc was conducted using HEK293F cells as described (Subedi et al. 2015).

NMR spectroscopy

NMR spectrometers operating at 21.1 T, 14.1 T (both Varian VNMRS) or 18.8 T, 16.4 T (Bruker Avance 3, Avance 2, respectively) were equipped with cryogenically-cooled 5 mm probes. ^{1}H resonance frequencies were internally referenced to DSS; ^{13}C and ^{15}N frequencies were indirectly referenced using the spectrometer's ^{1}H frequency at 0 ppm (Markley et al. 1998). NMR data were analyzed using Topspin (Bruker; v.2.1), NMRPipe (Delaglio et al. 1995), NMRViewJ (Johnson and Blevins 1994) and Sparky (version 3.115; Goddard and Kneller, University of California, San Francisco).

Assignment of ^{1}H–^{15}N correlation peaks collected using the variant *A*:Lu^{3+} chelate was completed as previously described (Barb et al. 2012) using triple resonance HNCO, HNCA, HNCACB and CBCACONH experiments collected at 14.1T and 10 °C (Cavanagh 2007). Assignments for variant *A* were deposited in the BioMagResBank (BMRB) as accession number 19769. Assignment of residues from the paramagnetic complexes (+Dy^{3+}

or + Tb^{3+}) were made by comparison to a spectrum of the corresponding diamagnetic complex (+Lu^{3+}) and using available backbone resonance assignment data of diamagnetic proteins where applicable [Z-l2LBT (BMRB 18126); variant *A* (19769); IgG1 Fc (25224)].

NMR spectra to probe the binding of variant *A* to IgG1 Fc were collected at 16.4 T and 50 °C. ^{1}H–^{15}N heteronuclear single quantum coherence (HSQC) spectra of isotopically enriched IgG1-Fc (150 μM: dimer) with selective [^{15}N]-Tyr amino acid residues were collected with and without variant *A* (330 μM) plus Lu^{3+} (330 μM). NMR samples were prepared in 25 mM MOPS, 100 mM sodium chloride, 0.5 mM DSS and 5 % D_2O, pH 7.2.

Measurements of *A* and *B* alignments were made with samples containing 150 μM protein with one molar equivalent of either Lu^{3+} or Dy $^{3+}$ at 25 °C and 21.1 T. NMR spectra to record pseudo-contact shifts (PCS) and residual dipolar coupling measurements (RDCs) on the IgG1 Fc:(variant *A*:Ln^{3+})$_2$ complex were collected at 18.8 T and 50 °C using 125 μM IgG1 Fc (dimer), 275 μM TEV-cleaved variant *A*, 290 μM Tb^{3+}(or Lu^{3+}) in a buffer containing 10 mM MOPS, 100 mM KCl, 0.5 mM DSS and 5 % D_2O, pH 7.2. RDCs were measured with a *J*-modulation based strategy as described (Barb et al. 2012; Liu and Prestegard 2009) by subtracting ^{1}H–^{15}N couplings measured with diamagnetic samples (containing the diamagnetic Lu^{3+} ion) from couplings measured with paramagnetic samples (containing the Tb^{3+}) and analyzed as described using PALES (Zweckstetter and Bax 2000). PCS were analyzed using NUMBAT (Schmitz et al. 2008).

Structure figures were prepared using PyMol (The PyMOL Molecular Graphics System, Version 1.5.0.4 Schrödinger, LLC).

Results and discussion

Lanthanide-binding properties of truncated Z-l2LBT variants

Z-l2LBT was targeted for optimization to reduce LBT motion relative to the three Z-domain helices. We designed two variants by eliminating amino acid residues in the two segments connecting the LBT and Z moieties that were believed to facilitate LBT mobility (Barb et al. 2012). Variant *A* (5 residues removed) and variant *B* (2 residues removed) expressed as soluble proteins at high yields using *E. coli* (>100 mg protein/L culture) and were purified (Fig. 1).

Variants *A* and *B* bound Tb^{3+} with high affinity in a spectrofluorophotometric assay that excites only polypeptide-bound ions at 280 nm through a Tyr residue in the LBT moiety. Titrating variant *A* or *B* with Tb^{3+} led to saturation of luminescence at 490 and 540 nm and is shown in Fig. 2. Variants *A* (700 ± 50 nM) and *B* (130 ± 50 nM) bound with dissociation constants (K_d) that are comparable to that of the original Z-l2LBT protein [130 ± 30 nM (Barb et al. 2012)]. As a result of the lanthanide ion binding affinity, either variant will be saturated at a ratio of 1:1 in NMR experiments that typically use >50 μM protein.

Domain motion of the lanthanide-binding Z-l2LBT variants

We estimated field-induced alignments of the Z domain moiety for the *A*:Dy^{3+} and *B*:Dy^{3+} complexes by measuring RDCs. If the Dy^{3+}:LBT moieties of each variant are assumed to align in an identical manner, a reasonable assumption due to complete conservation of the lanthanide-binding residues, principle alignment tensors (Da) fitted by analyzing RDCs of the underlying Z domains may be compared between variants as a relative measurement of Z domain alignment and thus interdomain LBT/Z mobility. This approach does not require the underlying Z-domains to align in the same orientation and was utilized here because the LBT residues were broadened beyond detection due to the paramagnetic ion, eliminating the possibility of measuring the amplitude of interdomain motion directly using RDCs.

HSQC spectra of ^{15}N-labeled variant *A*, variant *B* and Z-l2LBT with a 1 molar equivalent of Dy^{3+} were compared to spectra of diamagnetic Lu^{3+} complexes as shown in Fig. 3. The spectrum of variant *A* was affected substantially by PREs in the Dy^{3+} complex with only 14 amide peaks visible. A spectrum of variant *B* + Dy^{3+}, like the parent Z-l2LBT + Dy^{3+} complex, contained more than twice as many peaks as *A*. All three spectra showed the effect of PCSs (>0.5 ppm) (the Z-l2LBT spectrum is shown in Barb et al. 2012).

A comparison of the one-bond scalar ^{15}N–H coupling ($^{1}J_{NH}$) from the unassigned spectra of the designed proteins

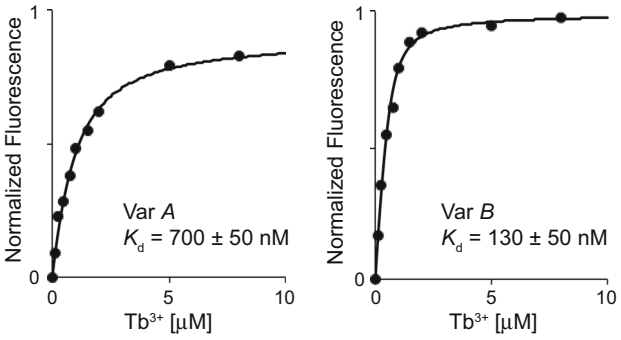

Fig. 2 Tb^{3+}-binding affinity of variants *A* and *B*

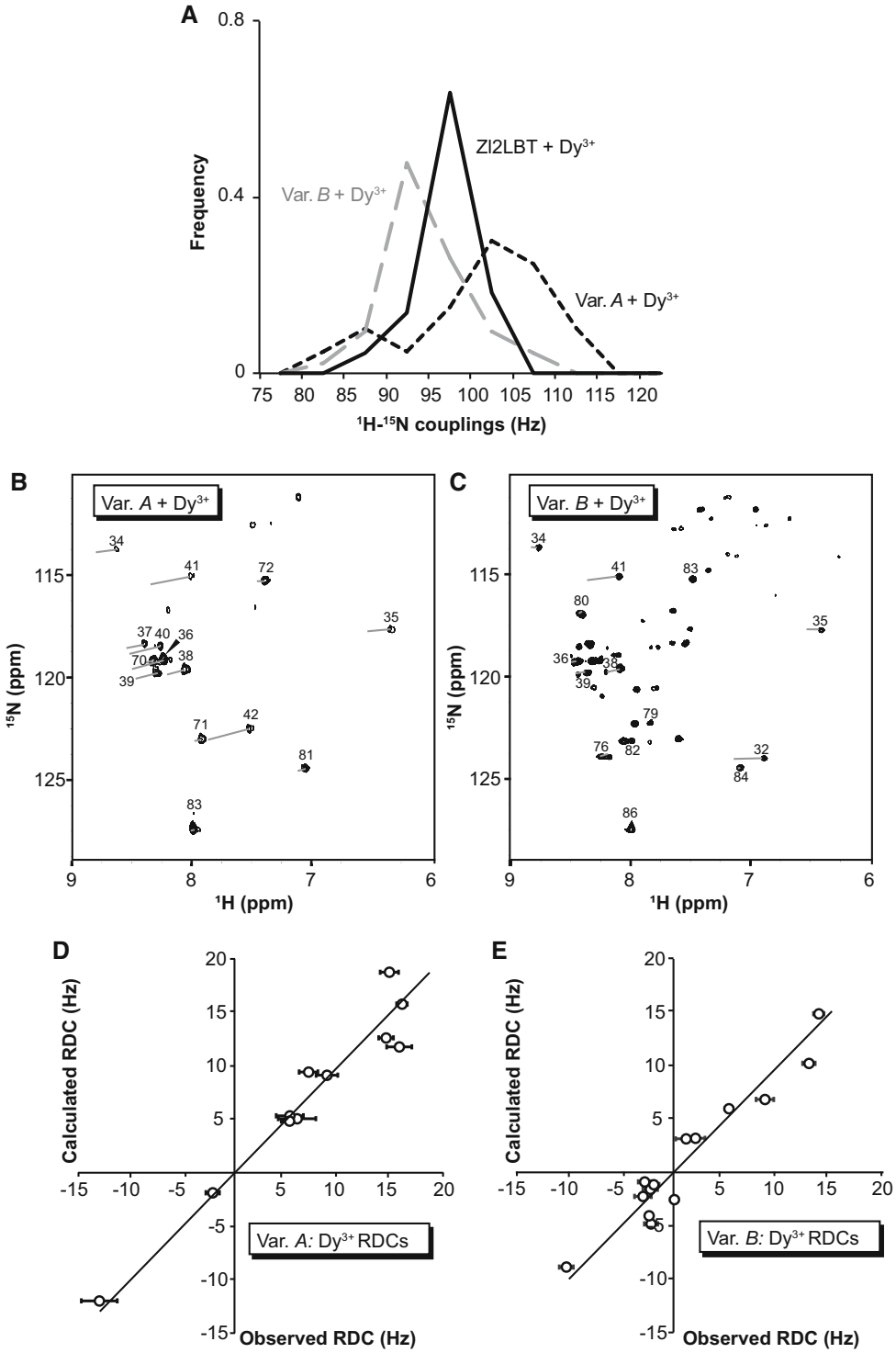

Fig. 3 RDCs of the designed proteins. **a** The distribution of one-bond $^{1}H–^{15}N$ coupling values for variants *A, B*, and Z-l2LBT was measured using unassigned peaks in the presence of Dy^{3+} at 21.1 T. **b**, **c** ^{15}N HSQC spectra of variants *A* and *B*, respectively, in complex with Dy^{3+}. Pseudo-contact shifts (PCSs) of assigned resonances are shown with a *grey line* with the origin corresponding to the position in the spectrum collected in the presence of Lu^{3+}. *Errors bars* represent the residue-specific sum of errors for individual fits of the Lu^{3+} and Dy^{3+} $^{15}N–H$ coupling observations. **d**, **e** Plots showing the observed RDC values of the *A*:Dy^{3+} and *B*:Dy^{3+} complexes versus the calculated values. The *line* represents $y = x$

in a Dy^{3+} complex provided insight into the different molecular properties. Variant *A* displayed the largest range of values (81–114 Hz) while the range of *B* (85–109 Hz) was less than *A* but greater than Z-l2LBT (88–103 Hz) as shown in Fig. 3a. The greater range of $^{1}J_{NH}$ values and fewer peaks resulting from PREs observed for *A* is consistent with an LBT that is closer to the three Z domain helices and experiences a reduced amplitude of motion.

Measurements of residual $^{1}H–^{15}N$ dipolar couplings for variant *A*, variant *B* and Z-l2LBT with one molar equivalent of Dy^{3+} provided an estimate of LBT motion for the three proteins (Fig. 3a). Peaks from *A* + Dy^{3+} (11) and

$B + Dy^{3+}$ (14) were assigned with high confidence and used for further analysis as shown in Fig. 3b, c. Alignment tensors (Da) fitted to the RDCs using a model of the Z-domain [pdb 1q2n (Zheng et al. 2004)] were qualitatively consistent with the ranges of $^{1}H–^{15}N$ coupling values (Table 1; Fig. 3a, d, e). Though only a limited number of assigned residues are visible in spectra collected in the presence of Dy^{3+}, these data do provide a means to estimate the motion of each LBT relative to the Z domain helices. The LBT of *A* and *B* experience a range of motion that is estimated to be 0.39 and 0.68 times that of Z-l2LBT, respectively, based on the tensor magnitude. A previous analysis found Z-l2LBT exhibited 40° of interdomain motion using a diffusion-in-a-cone model (Barb et al. 2012; Barbato et al. 1992). By comparison variants *A* and *B* exhibited ~16° and 27° of motion, respectively. This analysis, though a simplification that assumes motion is equally distributed within a cone, is informative as a singular estimate of relative mobility between the LBT and Z moieties.

Structural assessment of Z-l2LBT variants

The structural features of these proteins were probed by solution NMR spectroscopy. Both variants *A* and *B* appeared folded and experienced conformational rearrangements upon binding a diamagnetic Lu^{3+} ion based on two-dimensional $^{1}H–^{15}N$ HSQC spectra of variants *A* and *B*, before and after titrating Lu^{3+} (Fig. 4). Previous results indicate a significant change in Z-l2LBT conformation upon lanthanide binding is likely limited to the LBT moiety (Barb et al. 2012). Due to the large proportion of the structured protein formed by the LBT (21–23 %) and central location it is anticipated that lanthanide binding will induce noticeable chemical shift changes in a majority of the protein as observed (Fig. 4). The designed proteins exchanged between lanthanide bound and unbound states in the slow regime of the NMR timescale (data not shown).

A complete backbone resonance assignment of variant *A* assigned all major peaks observed in an $^{1}H–^{15}N$ HSQC spectrum (88 % of HN assigned, 89 % N, 79 % CA, 76 % CB, and 73 % CO from residues 13–83; Fig. 4c) and was consistent with a high degree of structural similarity to the parent Z-l2LBT protein. The high degree of structural similarity is supported by identical functional roles that are dependent upon structure, namely effective Tb^{3+} binding (discussed above) and antibody binding (discussed below). A few residues from loops connecting LBT to helices 2 & 3 plus a few residues from the middle of helix 3 were not observed (Fig. 1c).

NMR characterization of the A:Fc complex

We probed binding of variant *A* to IgG1 Fc in order to characterize the effects of two paramagnetic ions in the 72.2 kDa IgG1 Fc:(variant *A*:Tb^{3+})$_2$ complex (IgG1 Fc is a homodimer with two Z domain binding sites, see Fig. 1b). To reduce the rotational correlation time of the five-component complex and increase sensitivity as much as possible, a variant *A* form was prepared with a TEV-cleavable 6xHis tag. This variant was shown to bind Tb^{3+} with the same high affinity as the variant *A* construct containing a 6xHis tag and the TEV-cleaved form was utilized for subsequent experiments (data not shown).

A comparison of IgG1 Fc spectra before and after the addition of the variant *A*:Lu^{3+} chelate revealed the formation of a tightly bound complex as expected based on affinity of the Z domain for IgG1 Fc (Fig. 5) (Barb et al. 2012; Starovasnik et al. 1997). Two IgG1 Fc Tyr crosspeaks shifted as a result of complex formation; Tyr436 is proximal to the Z/Fc interface and experienced a large displacement (Deisenhofer 1981; DeLano et al. 2000). The Tyr373 crosspeak shifted slightly. The remaining six crosspeaks remained in the same spectral position but were slightly less intense likely due to an increase in the rotational correlation time upon variant *A* binding.

Paramagnetic effects of variant A in complex with Fc

Strong paramagnetic effects were observed in the IgG1 Fc:(variant *A*:Tb^{3+})$_2$ complex. Though significant PREs broadened many signals including K248, K288 and K320 as shown in Fig. 6, we focused on PCSs and field-induced RDCs of the Fc that indicate structural restriction of the LBT. The presence of PREs is not a good measure of structural restriction because these can be strong even if the

Table 1 RDC alignment parameters for Z-l2LBT, and variants *A* and *B* in complex with Dy^{3+} at 21.1T

Protein	# Obs	Da	Dr	Theoretical max coupling (Hz)	Q-value (Cornilescu et al. 1998)
Z-l2LBT	20	2.9×10^{-4}	9.0×10^{-5}	6.2	0.317
Variant *B*	14	4.2×10^{-4}	2.5×10^{-4}	9.1	0.261
Variant *A*	11	7.3×10^{-4}	4.2×10^{-4}	15.8	0.178

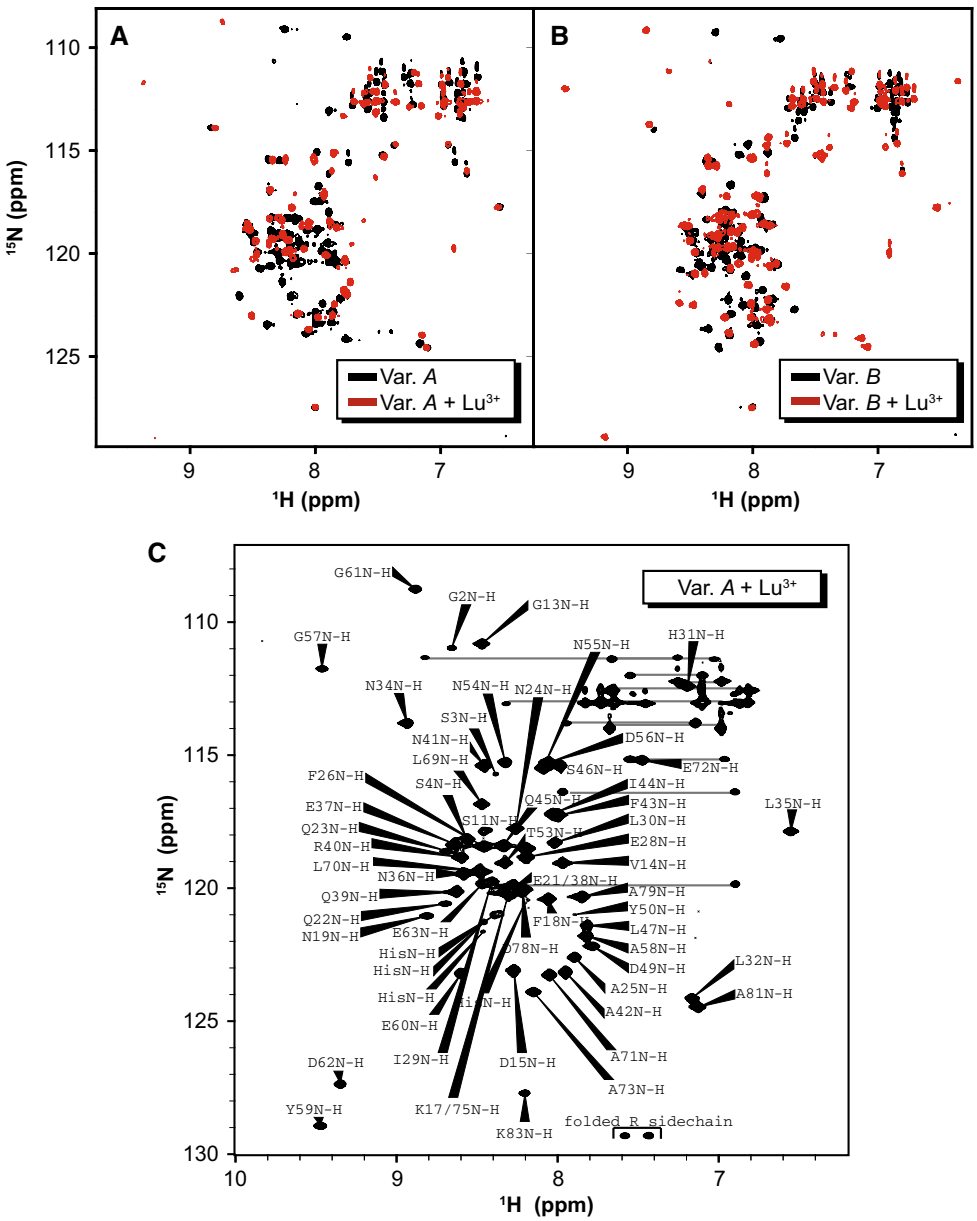

Fig. 4 2d NMR spectroscopy of variants *A* and *B*. ^{15}N-HSQC spectra of variants *A* (**a**) and *B* (**b**) before and after addition of Lu^{3+} at 25 °C reveal large changes in protein conformation. **c** Backbone amide crosspeaks of the variant *A*:Lu^{3+} complex were assigned with standard triple-resonance experiments collected at 10 °C. Sidechain amides are identified with horizontal *grey lines*

tag experiences a high degree of mobility relative to the underlying protein.

Substantial ^{1}H PCSs were observed in an ^{15}N-HSQC-TROSY spectrum of the IgG1 Fc:(variant *A*:Tb^{3+})$_2$ complex when compared to the Lu^{3+}-bound complex (Fig. 6). Of 21 assignable cross peaks from the Tb^{3+}-bound complex, 20 showed measureable PCSs between −0.221 and 0.081 ppm indicating the LBT tag was stabilized in a position to influence IgG1 Fc resonances. A small degree of heterogeneity is observed with some peaks, including Y436. It is unclear whether the LBT, lanthanide, or Fc contributes to this heterogeneity. A comparison of all observed PCSs with PCSs calculated using a structural model of the Fc monomer [pdb- 1L6X (DeLano et al. 2000)] revealed a high degree of similarity (Fig. 6b, the coefficient of determination squared (R^2) = 0.978).

That the PCSs fit the known structure with a high degree of similarity is important for three reasons. First, the Tb^{3+} ion is coordinated near the Fc protein and experiences limited motion, if any, relative to the Fc. Second, the ion is

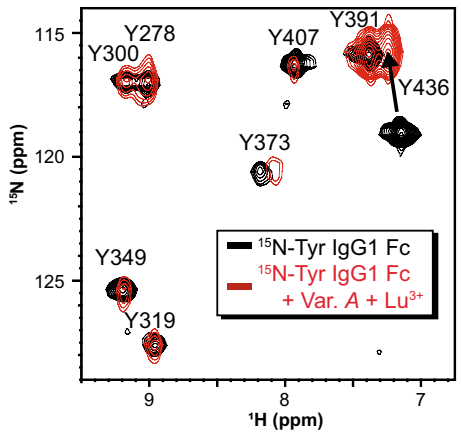

Fig. 5 ^{15}N-HSQC spectra of [^{15}N-Tyr]-IgG1 Fc collected at 16.4 T before and after addition of two molar equivalents of variant *A* and Lu^{3+}. Amino acid assignments are based on a published report (Matsumiya et al. 2007)

positioned in a manner that preferentially impacts resonances on the nearest monomer, and minimally affects the more distant Fc monomer in the Fc dimer. Third, these data confirm that the 1L6X structural model is a good representation of the Fc conformation in complex with the Z domain and supports recent solution measurements of Fc quaternary structure in solution (Subedi and Barb 2015).

We also pursued RDCs as a measurement of field-induced IgG1 Fc:(variant *A*:Tb^{3+})$_2$ alignment. We observed six RDCs with a range of −7.6 to 14.3 Hz and error <2.3 Hz (Table 2; Fig. 7). The smaller number of RDCs with low errors (6) with respect to PCS observations (20) reflects the effect of PREs on signal intensity in the *J*-modulation experiments that led to increased errors with the Tb^{3+} sample. These presence of RDCs is further strong evidence for conformational stability of the variant *A* LBT tag in the IgG1 Fc complex.

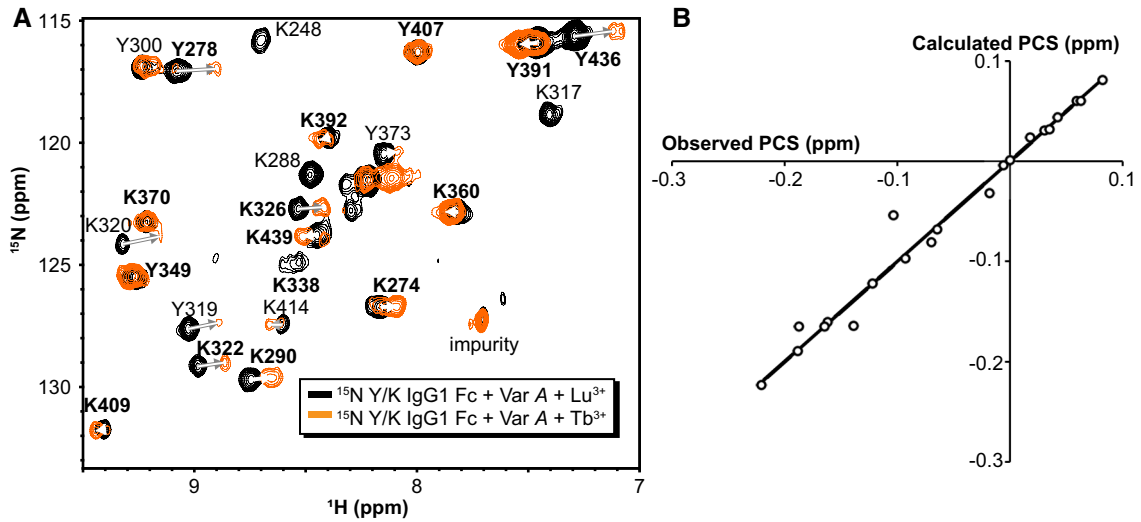

Fig. 6 Pseudo-contact shifts (PCSs) were detected among the [^{15}N-Tyr/Lys]-IgG1 Fc amide resonances at 18.8 T. **a** An overlay of ^{15}N-HSQC-TROSY spectra collected using the IgG1 Fc(Z-l2LBT:Lu^{3+})$_2$ and IgG1 Fc(Z-l2LBT:Tb^{3+})$_2$ complexes are shown in *black* and *orange* contours, respectively. Significant differences in resonance frequencies are denoted with *white and grey arrows*. **b** The observed ^{1}H PCSs correlate strongly to ^{1}H PCSs calculated by the NUMBAT program (Schmitz et al. 2008), using a model of the Fc protein determined by X-ray crystallography (DeLano et al. 2000). A *line* corresponding to the function y = x is shown in *black*

Table 2 Field-induced RDCs from IgG1 Fc residues in the IgG1 Fc:(variant *A*:Tb^{3+})$_2$ complex

Residue	Coupling with Lu^{3+} (Hz)	Error (Hz)	Coupling with Tb^{3+} (Hz)	Error (Hz)	RDC (Hz)
K290	92.4	1.4	106.7	2.2	14.3
Y349	97.2	1.2	95.3	1.5	−1.9
K360	95.7	2.1	88.1	0.8	−7.6
Y391	96.0	2.0	94.9	1.3	−1.1
K392	97.4	2.3	105.9	2.2	8.5
Y407	95.8	2.3	100.4	0.8	4.6

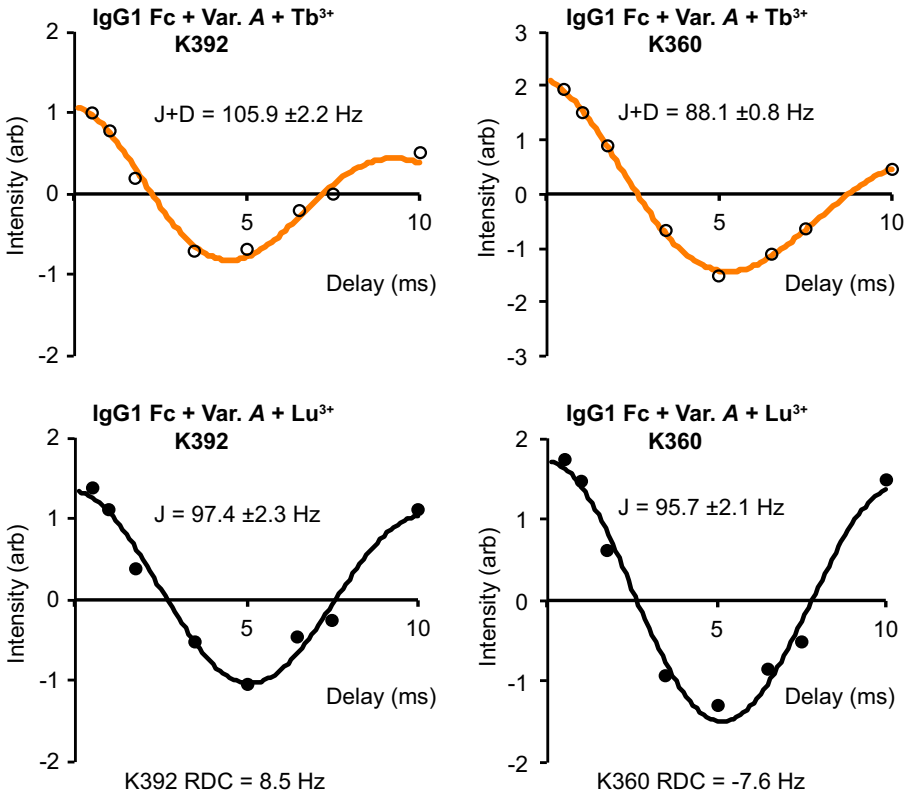

Fig. 7 Residual dipolar couplings (RDCs) of the Fc amide resonances were identified using the IgG1 Fc(Var. *A*:Tb^{3+})$_2$ complex. Spectra collected using isotropic (*black line* with *black circles*; complex with Lu^{3+}) and partially aligned (*orange line* with *open circles*; complex with Tb^{3+}) conditions at 18.8 T revealed significant positive and negative RDCs using a *J*-modulation method to measure ^{1}H–^{15}N couplings (Liu and Prestegard 2009)

Conclusions

Here we detailed the modification of a chimeric lanthanide and IgG1 binding protein to dramatically reduce the size and mobility of the metal binding moiety. This redesigned LBT tag is widely applicable to other structure-based investigations and has been utilized to study the two-domain SpA-N protein (Prof. T. Oas, Duke University), a two-domain roundabout (ROBO) family construct and a fragment of the extracellular domains of a leukocyte common antigen-related receptor protein tyrosine phosphatase (Prof. K. Moremen, UGA). We demonstrated the utility of one new design to investigate the structure of a large 72.2 kDa complex. These shortened LBTs provide one approach to reducing the motion of LBTs in many other protein systems that require limited LBT motion.

Acknowledgments We thank Prof. James H. Prestegard (CCRC, UGA) for helpful suggestions throughout this project and use of the 21.1 T and 14.1 T spectrometers, Dr. D. Bruce Fulton (ISU) for help with NMR experiments, Prof. Vincenzo Venditti (ISU) for a critical reading of the manuscript and the Roy J. Carver Charitable Trust (Muscatine, IA) for supporting scientific instrumentation. This work was financially supported by the grant R01-GM115489 from the National Institutes of Health and the Roy J. Carver Department of Biochemistry, Biophysics & Molecular Biology at Iowa State University. The content of this work is solely the responsibility of the authors and does not necessarily represent the official views of the NIH or ISU.

References

Barb AW, Ho TG, Flanagan-Steet H, Prestegard JH (2012) Lanthanide binding and IgG affinity construct: potential applications in solution NMR, MRI, and luminescence microscopy. Protein Sci 21:1456–1466. doi:10.1002/pro.2133

Barbato G, Ikura M, Kay LE, Pastor RW, Bax A (1992) Backbone dynamics of calmodulin studied by 15 N relaxation using inverse detected two-dimensional NMR spectroscopy: the central helix is flexible. Biochemistry 31:5269–5278

Barthelmes K et al (2011) Engineering encodable lanthanide-binding tags into loop regions of proteins. J Am Chem Soc 133:808–819. doi:10.1021/ja104983t

Bertini I, Luchinat C, Parigi G (2002) Paramagnetic constraints: an aid for quick solution structure determination of paramagnetic metalloproteins. Concepts Magn Reson 14:259–286. doi:10.1002/Cmr.10027

Butler A (1998) Vanadium haloperoxidases. Curr Opin Chem Biol 2:279–285

Cavanagh J (2007) Protein NMR spectroscopy: principles and practice, 2nd edn. Academic Press, Boston, Amsterdam

Cornilescu G, Marquardt JL, Ottiger M, Bax A (1998) Validation of protein structure from anisotropic carbonyl chemical shifts in a dilute liquid crystalline phase. J Am Chem Soc 120:6836–6837

Deisenhofer J (1981) Crystallographic refinement and atomic models of a human Fc fragment and its complex with fragment B of protein A from Staphylococcus aureus at 2.9- and 2.8-A resolution. Biochemistry 20:2361–2370

Delaglio F, Grzesiek S, Vuister GW, Zhu G, Pfeifer J, Bax A (1995) NMRPipe: a multidimensional spectral processing system based on UNIX pipes. J Biomol NMR 6:277–293

DeLano WL, Ultsch MH, de Vos AM, Wells JA (2000) Convergent solutions to binding at a protein-protein interface. Science 287:1279–1283

Feeney J, Birdsall B, Bradbury AF, Biekofsky RR, Bayley PM (2001) Calmodulin tagging provides a general method of using lanthanide induced magnetic field orientation to observe residual dipolar couplings in proteins in solution. J Biomol NMR 21:41–48. doi:10.1023/A:1011924017938

Gaponenko V, Dvoretsky A, Walsby C, Hoffman BM, Rosevear PR (2000) Calculation of z-coordinates and orientational restraints using a metal binding tag. Biochemistry 39:15217–15224

Hanson QM, Barb AW (2015) A perspective on the structure and receptor binding properties of immunoglobulin G Fc. Biochemistry 54:2931–2942. doi:10.1021/acs.biochem.5b00299

Hiruma Y et al (2013) The structure of the cytochrome p450cam-putidaredoxin complex determined by paramagnetic NMR spectroscopy and crystallography. J Mol Biol 425:4353–4365. doi:10.1016/j.jmb.2013.07.006

Huang F, Pei Y-Y, Zuo H-H, Chen J-L, Yang Y, Su X-C (2013) Bioconjugation of proteins with a paramagnetic NMR and fluorescent tag. Chem Eur J 19:17141–17149. doi:10.1002/chem.201302273

Iwahara J, Clore GM (2006) Detecting transient intermediates in macromolecular binding by paramagnetic NMR. Nature 440:1227–1230. doi:10.1038/nature04673

Iwahara J, Schwieters CD, Clore GM (2004a) Characterization of nonspecific protein-DNA interactions by 1H paramagnetic relaxation enhancement. J Am Chem Soc 126:12800–12808. doi:10.1021/ja046246b

Iwahara J, Schwieters CD, Clore GM (2004b) Ensemble approach for NMR structure refinement against (1)H paramagnetic relaxation enhancement data arising from a flexible paramagnetic group attached to a macromolecule. J Am Chem Soc 126:5879–5896. doi:10.1021/ja031580d

Johnson BA, Blevins RA (1994) NMR view: a computer-program for the visualization and analysis of NMR data. J Biomol NMR 4:603–614

Keniry MA, Park AY, Owen EA, Hamdan SM, Pintacuda G, Otting G, Dixon NE (2006) Structure of the theta subunit of *Escherichia coli* DNA polymerase III in complex with the epsilon subunit. J Bacteriol 188:4464–4473. doi:10.1128/JB.01992-05

Koehler J, Meiler J (2011) Expanding the utility of NMR restraints with paramagnetic compounds: background and practical aspects. Prog Nucl Magn Reson Spectrosc 59:360–389. doi:10.1016/j.pnmrs.2011.05.001

Lee MD et al (2015) Compact, hydrophilic, lanthanide-binding tags for paramagnetic NMR spectroscopy. Chem Sci 6:2614–2624. doi:10.1039/c4sc03892d

Liu Y, Prestegard JH (2009) Measurement of one and two bond N–C couplings in large proteins by TROSY-based J-modulation experiments. J Magn Reson 200:109–118. doi:10.1016/j.jmr.2009.06.010

Loh CT, Ozawa K, Tuck KL, Barlow N, Huber T, Otting G, Graham B (2013) Lanthanide tags for site-specific ligation to an unnatural amino acid and generation of pseudocontact shifts in proteins. Bioconj Chem 24:260–268. doi:10.1021/bc300631z

Loh C-T, Graham B, Abdelkader EH, Tuck KL, Otting G (2015) Generation of pseudocontact shifts in proteins with lanthanides using small "Clickable" nitrilotriacetic acid and iminodiacetic acid tags. Chem Eur J 21:5084–5092. doi:10.1002/chem.201406274

Markley JL et al (1998) Recommendations for the presentation of NMR structures of proteins and nucleic acids–IUPAC-IUBMB-IUPAB Inter-Union task group on the standardization of data bases of protein and nucleic acid structures determined by NMR spectroscopy. Eur J Biochem 256:1–15

Martin LJ, Imperiali B (2015) The best and the brightest: exploiting tryptophansensitized Tb3 + luminescence to engineer lanthanide-binding tags. In: Derda R (ed) Peptide libraries: methods and protocols, vol 1248. Methods in molecular biology. pp 201–220. doi:10.1007/978-1-4939-2020-4_14

Matsumiya S et al (2007) Structural comparison of fucosylated and nonfucosylated Fc fragments of human immunoglobulin G1. J Mol Biol 368:767–779. doi:10.1016/j.jmb.2007.02.034

Nilsson B et al (1987) A synthetic IgG-binding domain based on staphylococcal protein A. Protein Eng 1:107–113

Nitz M, Franz KJ, Maglathlin RL, Imperiali B (2003) A powerful combinatorial screen to identify high-affinity terbium(III)-binding peptides. ChemBioChem 4:272–276. doi:10.1002/cbic.200390047

Otting G (2008) Prospects for lanthanides in structural biology by NMR. J Biomol NMR 42:1–9. doi:10.1007/s10858-008-9256-0

Parekh RB et al (1985) Association of rheumatoid arthritis and primary osteoarthritis with changes in the glycosylation pattern of total serum IgG. Nature 316:452–457

Park SH, Wang VS, Radoicic J, De Angelis AA, Berkamp S, Opella SJ (2015) Paramagnetic relaxation enhancement of membrane proteins by incorporation of the metal-chelating unnatural amino acid 2-amino-3-(8-hydroxyquinolin-3-yl)propanoic acid (HQA). J Biomol NMR 61:185–196. doi:10.1007/s10858-014-9884-5

Pilla KB, Leman JK, Otting G, Huber T (2015) Capturing conformational states in proteins using sparse paramagnetic NMR data. PLoS ONE. doi:10.1371/journal.pone.0127053

Prestegard JH, Bougault CM, Kishore AI (2004) Residual dipolar couplings in structure determination of biomolecules. Chem Rev 104:3519–3540. doi:10.1021/Cr030419i

Saio T, Ogura K, Yokochi M, Kobashigawa Y, Inagaki F (2009) Two-point anchoring of a lanthanide-binding peptide to a target protein enhances the paramagnetic anisotropic effect. J Biomol NMR 44:157–166. doi:10.1007/s10858-009-9325-z

Schmitz C, Stanton-Cook MJ, Su XC, Otting G, Huber T (2008) Numbat: an interactive software tool for fitting Delta chi-tensors to molecular coordinates using pseudocontact shifts. J Biomol NMR 41:179–189. doi:10.1007/s10858-008-9249-z

Shulman RG, Wuthrich K, Yamane T, Antonini E, Brunori M (1969) Nuclear magnetic resonances of reconstituted myoglobins. Proc Natl Acad Sci USA 63:623–628

Silvaggi NR, Martin LJ, Schwalbe H, Imperiali B, Allen KN (2007) Double-lanthanide-binding tags for macromolecular crystallographic structure determination. J Am Chem Soc 129:7114–7120. doi:10.1021/ja070481n

Sjodt M et al (2015) The PRE-derived NMR model of the 38.8-kDa tri-domain IsdH protein from staphylococcus aureus suggests that it adaptively recognizes human hemoglobin. J Mol Biol. doi:10.1016/j.jmb.2015.02.008

Skinner SP, Liu W-M, Hiruma Y, Timmer M, Blok A, Hass MAS, Ubbink M (2015) Delicate conformational balance of the redox enzyme cytochrome P450cam. Proc Natl Acad Sci USA 112:9022–9027. doi:10.1073/pnas.1502351112

Starovasnik MA, Braisted AC, Wells JA (1997) Structural mimicry of a native protein by a minimized binding domain. Proc Natl Acad Sci USA 94:10080–10085

Su XC, Huber T, Dixon NE, Otting G (2006) Site-specific labelling of proteins with a rigid lanthanide-binding tag. ChemBioChem 7:1599–1604. doi:10.1002/cbic.200600142

Su XC, McAndrew K, Huber T, Otting G (2008) Lanthanide-binding peptides for NMR measurements of residual dipolar couplings and paramagnetic effects from multiple angles. J Am Chem Soc 130:1681–1687. doi:10.1021/ja076564l

Subedi GP, Barb AW (2015) The structural role of antibody N-glycosylation in receptor interactions. Structure 23:1573–1583. doi:10.1016/j.str.2015.06.015

Subedi GP, Moniz HA, Johnson RW, Moremen KW, Barb AW (2015) High yield expression of recombinant human proteins with the transient transfection of HEK293 cells in suspension JoVE (in press)

Tashiro M, Tejero R, Zimmerman DE, Celda B, Nilsson B, Montelione GT (1997) High-resolution solution NMR structure of the Z domain of staphylococcal protein A. J Mol Biol 272:573–590. doi:10.1006/jmbi.1997.1265

Tolman JR, Flanagan JM, Kennedy MA, Prestegard JH (1995) Nuclear magnetic dipole interactions in field-oriented proteins: information for structure determination in solution. Proc Natl Acad Sci USA 92:9279–9283

Wei Z, Yang Y, Li Q-F, Huang F, Zuo H-H, Su X-C (2013) Noncovalent tagging proteins with paramagnetic lanthanide complexes for protein study. Chem Eur J 19:5758–5764. doi:10.1002/chem.201204152

Yagi H, Pilla KB, Maleckis A, Graham B, Huber T, Otting G (2013) Three-dimensional protein fold determination from backbone amide pseudocontact shifts generated by lanthanide tags at multiple sites. Structure 21:883–890. doi:10.1016/j.str.2013.04.001

Yang Y, Wang J-T, Pei Y-Y, Su X-C (2015) Site-specific tagging proteins via a rigid, stable and short thiolether tether for paramagnetic spectroscopic analysis. Chem Commun 51:2824–2827. doi:10.1039/c4cc08493d

Zheng D, Aramini JM, Montelione GT (2004) Validation of helical tilt angles in the solution NMR structure of the Z domain of Staphylococcal protein A by combined analysis of residual dipolar coupling and NOE data. Protein Sci 13:549–554. doi:10.1110/ps.03351704

Zweckstetter M, Bax A (2000) Prediction of sterically induced alignment in a dilute liquid crystalline phase: aid to protein structure determination by NMR. J Am Chem Soc 122:3791–3792. doi:10.1021/Ja0000908